Microchannel plates for the UVCS and SUMER instruments on the SOHO satellite

O. H. W. Siegmund, M. A. Gummin, T. Sasseen, P. Jelinsky, G. A. Gaines, J. Hull, J. M. Stock, M. Edgar, B. Welsh, S. Jelinsky, and J. Vallerga

Space Sciences Laboratory, University of California, Berkeley, CA 94720

1. ABSTRACT

The microchannel plates for the detectors in the SUMER[1] and UVCS[1] instruments aboard the Solar Orbiting Heliospheric Observatory[1] (SOHO) mission to be launched in late 1995 are described. A low resistance Z stack of microchannel plates (MCP's) is employed in a detector format of 27mm x 10mm using a multilayer cross delay line anode (XDL) with 1024 x 360 digitized pixels. The MCP stacks provide gains of $>2 \times 10^7$ with good pulse height distributions (as low as 25% FWHM) under uniform flood illumination. Background rates of ≈0.6 event cm^{-2} sec^{-1} are obtained for this configuration. Local counting rates up to ≈800 events/pixel/sec have been achieved with little drop of the MCP gain. MCP preconditioning results are discussed, showing that some MCP stacks fail to have gain deacreases when subjected to a high flux UV scrub. Also, although the bare MCP quantum efficiencies are close to those expected (≈10%), we found that the long wavelength response of KBr photocathodes could be substantially enhanced by the MCP scrubbing process. Flat field images are characterised by a low level of MCP fixed pattern noise and are stable. Preliminary calibration results for the instruments are shown.

Keywords: microchannel plate, UV, spectroscopy

2. INSTRUMENT DESCRIPTIONS

The UVCS and SUMER are both spectroscopy experiments on the SOHO mission. The UVCS spectrograph will examine the solar corona out to ≈10 solar radii in the wavelength range 500 - 1300Å. UVCS has two wavelength channels with XDL detectors. One is optimized for the Lyman α region (1148Å - 1283Å), and the other for the O VI emission line region (932 - 1068Å), which also accomodates Si XII (499Å & 521Å) in second order. The spectral resolution, $\lambda/\delta\lambda$, is ≈10,000 (0.1Å). Determination of spectral line profiles and intensities will allow investigations of coronal heating, and solar wind acceleration and composition.

The SUMER spectrograph will examine regions of the solar atmosphere in the wavelength range 500 - 1600Å. The spectral resolution, $\lambda/\delta\lambda$, is ≈40,000 (0.04Å), with ≈40Å of the spectrum imaged at the detector at any given time. The spectral region for a specific observation may be selected by scanning the spectrum across the detector using a scan mirror. The SUMER spectrograph employs one primary detector and a secondary detector as a backup channel. Primary goals are the study of flows, turbulent motions, and temperatures and densities of the upper solar atmosphere.

The microchannel plates for the SOHO UVCS and SUMER detectors require high quantum detection efficiency (QDE) >7% @ 584Å (SUMER), counting rate capacity of >100 events sec^{-1} $pixel^{-1}$ (25μm), low fixed pattern noise, gain $>10^7$ with narrow pulse height distributions, long term stability and need to support spatial resolution of <25μm.

3. MICROCHANNEL PLATE & DETECTOR DESIGN

The flight detector configuration for both the SOHO UVCS and SUMER experiments is displayed in Fig. 1. and a photograph of the UVCS O VI detector is shown in Figure 2. The detector

0-8194-1877-3/95/$6.00

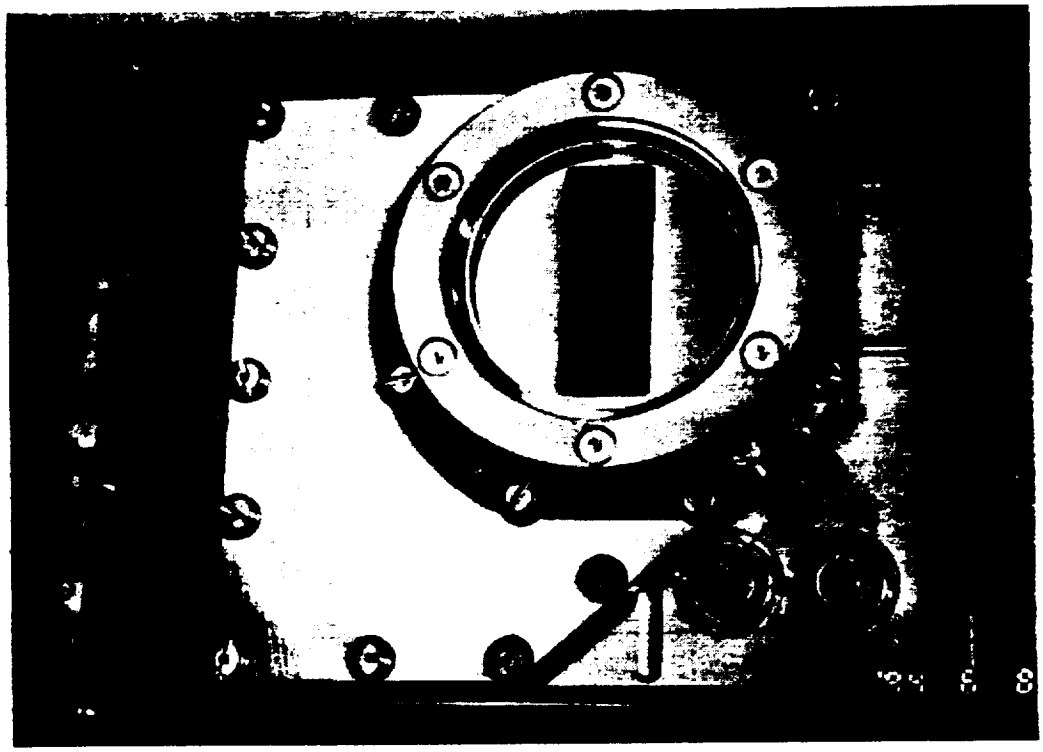

Figure 1. Photograph of the flight SOHO detector configuration showing the rectangular 10mm x 26mm field of view aperture, high voltage connectors and the vacuum flange.

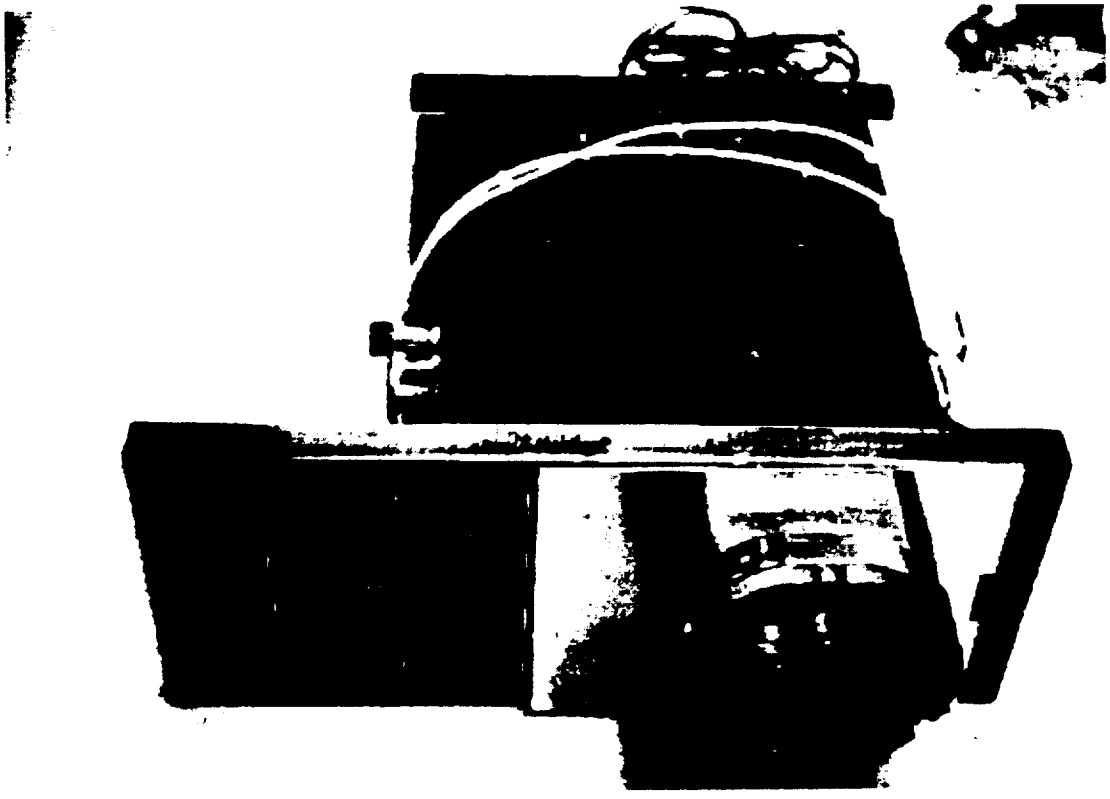

Figure 2. Photograph of the flight SOHO UVCS OVI detector on its flange with amplifiers and high voltage power supply

scheme is functionally similar to other devices that we have implemented in various space programs. An opaque KBr photocathode is deposited on a MCP Z stack, and incoming photons interact with the photocathode, resulting in photoelectron emission[2,3]. The photoelectrons impact the walls of MCP pores causing a charge avalanche, giving an overall charge multiplication of ≈2 x 10^7. This charge cloud is drifted from the MCP output to the XDL anode[4]. The charge is divided equally between the XDL charge collection fingers in the X (27mm) and Y (10mm) axes which are connected to X and Y external serpentine delay lines. X and Y photon event centroid positions are deduced from the signal arrival time differences at the two ends of each delay line. Image encoding electronics then provides the necessary processing for event position determination, and digitizes the X and Y event positions prior to data histogramming and telemetry to the ground.

The MCP's are mounted in a brazed metal-ceramic detector body providing ruggedness and low weight. The detector has a circumferential spring clamping arrangement for the MCP stack that has proven to be successful on a number of earlier flights[5]. The MCP scheme utilizes three 80:1 channel length/diameter (l/d) MCP's in a back to back "Z" stack. All the flight MCP's were obtained from Philips. The MCP's have 12.5μm pores (15μm spacing) with 13° bias angle, on a 36mm circular borderless format and resistance of ≈20MΩ per MCP. The field of view (27 x 10mm) is defined by an aperture mask placed in contact with the top MCP (Fig. 1). The brazed detector body is attached to a support plate (Fig. 1) that clamps the readout anode in place on the vacuum flange with a ≈7mm MCP to anode gap. The detector flange is made of titanium for low weight, and contains both signal and high voltage feedthroughs. There is a pumping port on the flange to allow purge and vacuum lines to be attach during various tests. Shown in Figure 2. are the vacuum housing which covers the detectors and the amplifier electronics box & high voltage power supply mounted to the detector flange. There is also a thermal ion rejection mesh covering the entrance aperture for the UVCS O-VI detector, and thermal ion electrostatic deflectors and meshes for attenuation of Ly α for both SUMER detectors.

4. Microchannel Plate Performance

4.1 Microchannel plate gain, pulse height distribution and background

Over 10 MCP Z stacks have been tested as part of the overall SOHO XDL detector development program. Although the results of these tests show variations in performance from stack to stack these differences have generally not been large. The pulse height spectra are gaussian in shape, and the widths at the operating gain are typically <50% FWHM under full flood illumination with a Hg vapor lamp (2537Å). The gain, pulse height and background results for the SUMER 1 detector are shown in Figures 3 and 4. For all the SOHO MCP's gains >2 x 10^7 have been achievable. The gain is not fully saturated at 2 x 10^7 however, and gains in excess of 4 x 10^7 were reached in some tests. The pulse height distributions for the SUMER 1 and 2 flight detectors were both particularly good, as indicated by the narrow distributions in Figures 3 and 4. This is an advantage for the discrimination of background events and setup of the electronics. The baseline below the peak of the pulse height distribution has almost no counts below 1 x 10^7. The background rate as a function of gain threshold for the SUMER 1 MCP's is also shown in Figure 3. This characteristic was derived from the pulse height distribution for backround events accumuated over a long integration time. If a threshold is applied at 1 x 10^7 the background rate drops to <0.4 events cm^{-2} $sec^{-1}$with no effect on the photon data. The overall background rate close to that expected for intrinsic β decay MCP noise[6,7] for ^{40}K in the Philips glass, with a rate of ≈0.65 events sec^{-1} uniformly distributed across the field of view. Typically the background rates measured were slightly higher than the intrinsic β decay rate because the detectors were normally uncovered and exposed to the entire test vacuum tank volume, resulting in a low rate of stray ion events at gains close to the model gain.

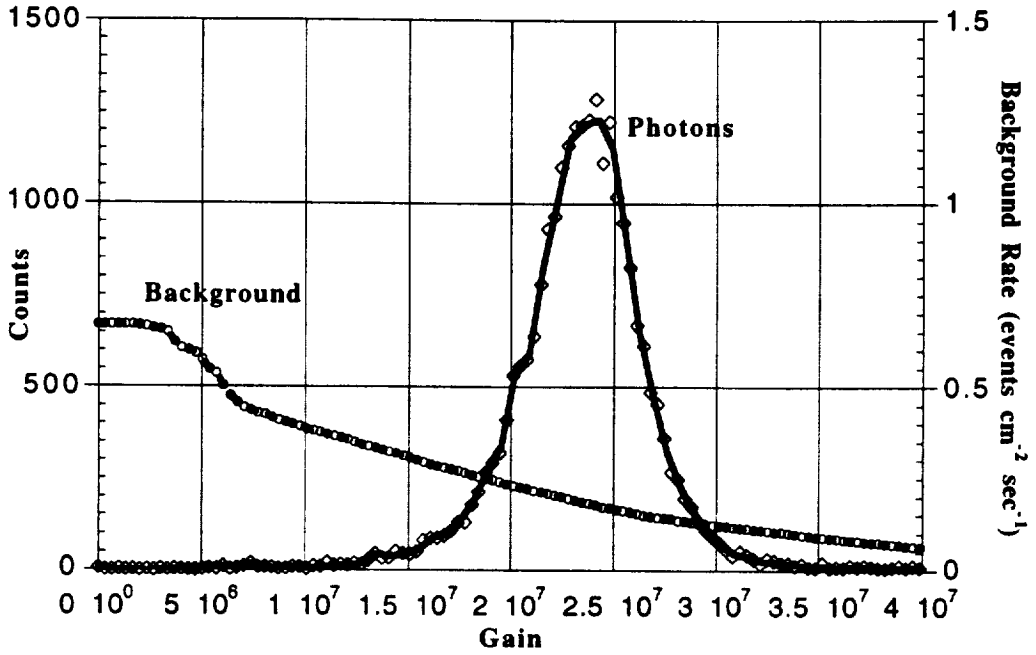

Figure 3. 2537Å light pulse height distribution for the SUMER 1 MCP's compared with the background rate as a function of gain threshold derived from the background event PHD.

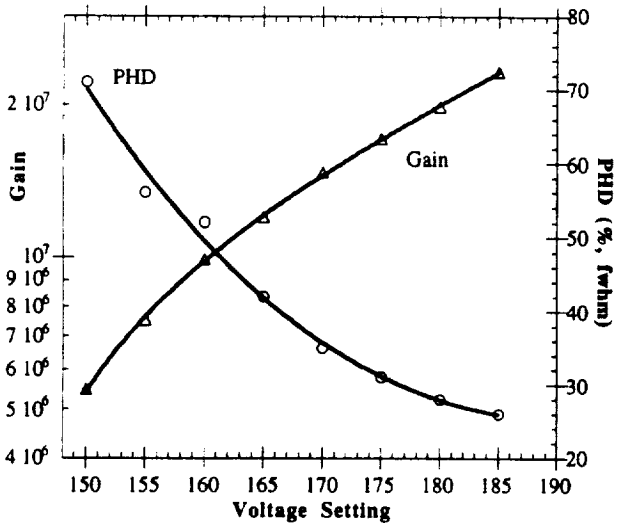

Figure 4. Gain and pulse height distribution characteristics for the flight SUMER 1 detector MCP's

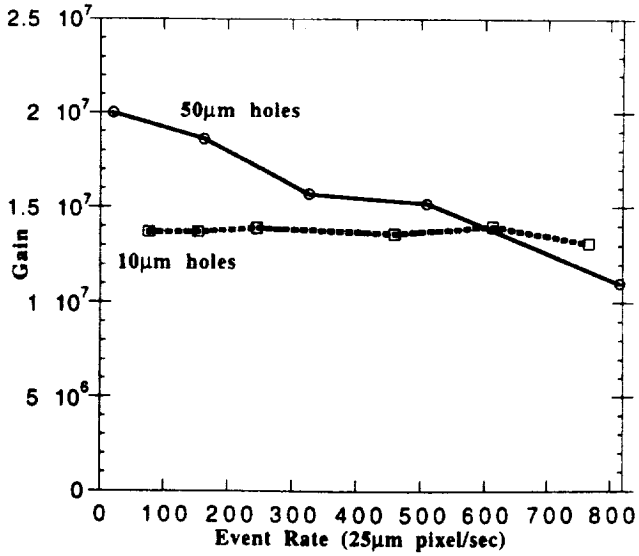

Figure 5. Gain as a function of local counting rate for small illuminated areas. SOHO flight MCP's.

Previous studies have found a progressive drop in the MCP stack gain and a degradation of the pulse amplitude distribution[8,9,10] due to the finite recharge time of MCP channel(s). The counting rate requirements of the SOHO UVCS and SUMER experiments are sufficiently high that low resistivity MCP's were chosen to preserve operational stability. The resistance values in the range 250MΩ/cm^2 were selected for the SOHO XDL MCP's (≈20MΩ per MCP). Tests were made to evaluate the high local counting rate conditions expected when high flux lines from the SOHO spectrographs are incident on the detectors. The high local counting rates on the MCP were generated using a variable flux from a pen ray lamp to illuminate pinhole masks with 10μm and 50μm pinholes. The gain as a function of local counting rate for one SOHO MCP set is shown in Figure 5. The results show that for these MCP's the gain remains stable up to ≈800 events pixel^{-1} sec^{-1}for the 10μm holes. For the 50μm holes the gain drop is only ≈20% up to 500 events pixel^{-1} sec^{-1}, which is acceptable for SOHO, causing no loss of events or resolution. The difference in behavior for the different sized illuminated areas is due to the contributions of the "reserve" charge in the MCP pores circumferential to the illuminated area[10]. In both measurement sets the performance is better than the requirements of SOHO.

4.2 Microchannel preconditioning

The preconditioning of the SOHO MCP's followed the same general procedures described by Siegmund[11]. The processing flow followed the sequence of cleaning, baking, depositing the KBr photocathode, and finally scrubbing the MCP stack. Each MCP used for the SOHO flight or ancillary test detectors was cleaned in a series of isopropyl and methyl alcohol ultrasonic baths and oven baked prior to assembling into a detector unit. After the detector assembly and initial MCP functional tests the detectors were vacuum baked at ≈120° C for 4-8 hours. This is somewhat less than normally used[11], but was necessitated by the fact that the vacuum flange was "o" ring sealed. Functional tests immediately after the bake gave gain, pulse height and background performance results that were statistically identical to the pre-bake values.

The photocathode was deposited following the bake according to the photocathode deposition procedure described in previous publications [2,3]. A point to note is that the UVCS detectors were completely coated with KBr but the SUMER detectors were only coated with KBr over the center 50% of the detector area. A high flux "burn in" or "scrub" to stabilize the overall MCP gain was performed immediately following the photocathode deposition for all flight detectors. The scrub setup illuminates the detector with light from a Hg vapor lamp. The principal UV emission lines from this lamp are at 1879Å and 2537Å. The detectors were operated during the scrub with an overall voltage ≈600 – 800 V below nominal operating range, providing a gain of ≈5 x 10^5 electrons photon^{-1}. The DC current from the MCP's was typically ≈1μA during the scrub, and the the total charge extracted was ≈0.05 – 0.1 C cm^{-2}.

The scrub behavior of the SOHO MCP's was unusual in that some MCP stacks did not show significant gain drop with charge extractions of up to ≈0.1 C cm^{-2}. Figures 6,7 & 8 show the pre– and post–scrub gain–voltage curves for the SOHO SUMER 1 and UVCS Lyα & O VI flight detectors. These show no significant gain drop following the scrub. Meanwhile Figure 9 shows more normal scrubbing behavior found for the SUMER 2 backup detector. The anomalous behavior is seen for scrubs performed at different times, for two different boules of MCP material, and on the MCP' areas both with and without photocathodes. In attempts to duplicate this behaviour we have scrubbed three other sets of SOHO MCP's, such as the one shown in Figure 10. In all cases the gain scrubbed down in a "normal" process. The decrease in gain during a scrub is generally thought to be due to a combination of depleting the gas adsorbed on the walls of the MCP pores, and changes in the physical structure of the channel plate wall[12]. At this point we have no consistent explanation for the phenomenon but continue to investigate possible reasons for this interesting MCP behavior.

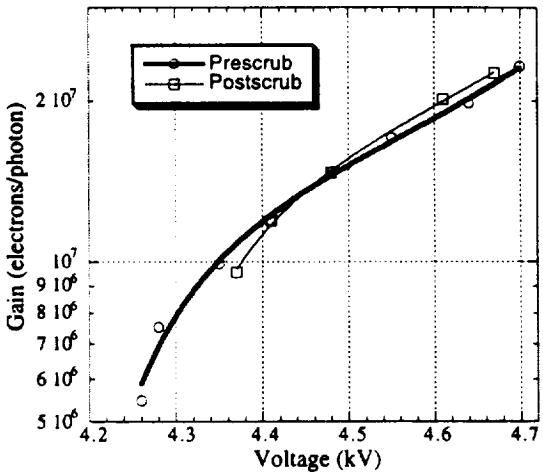

Figure 6. Before and after scrub gain curves for SUMER 1 flight detector, 0.088 C cm^{-2} scrub.

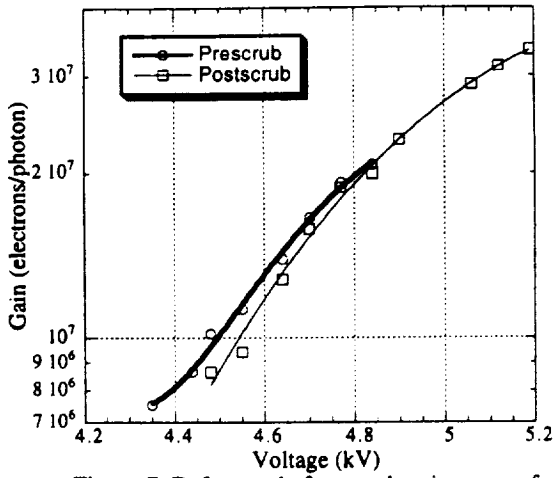

Figure 7. Before and after scrub gain curves for UVCS O VI flight detector, 0.071 C cm^{-2} scrub.

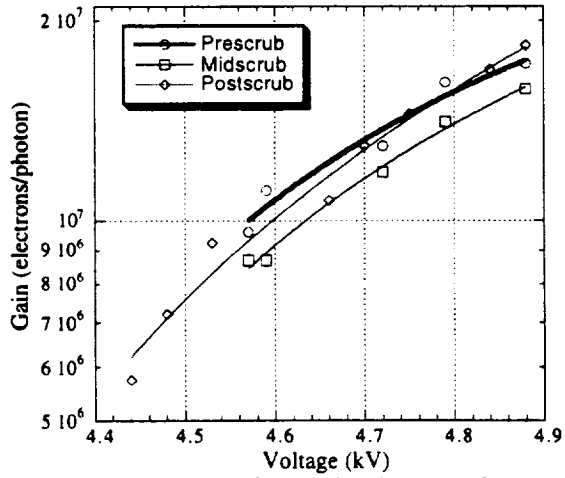

Figure 8. Before and after scrub gain curves for UVCS Lyα flight detector, 0.043 C cm^{-2} scrub.

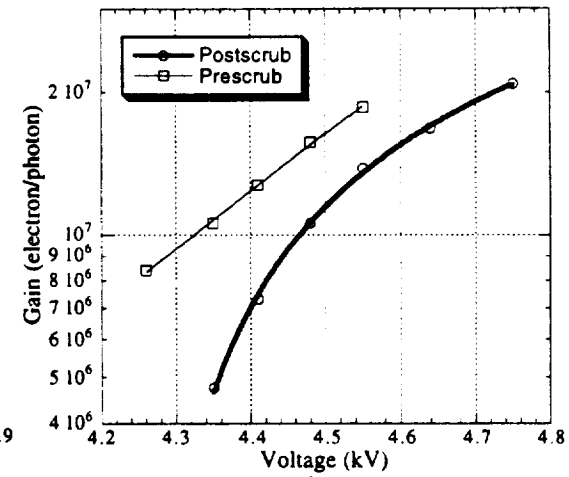

Figure 9. Before and after scrub gain curves for SUMER 2 backup detector, 0.08 C cm^{-2} scrub.

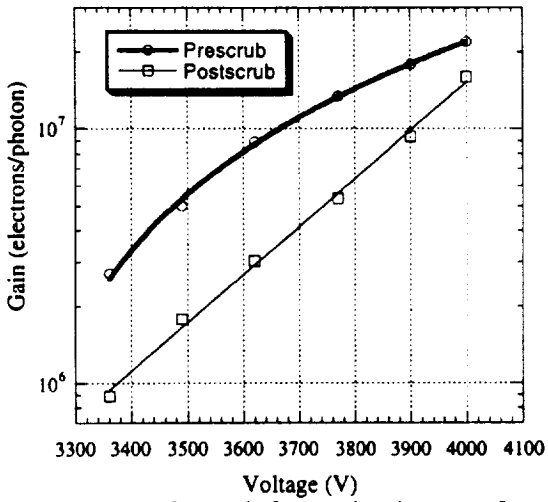

Figure 10. Before and after scrub gain curves for SOHO MCP test detector, 0.013 C cm^{-2} scrub.

4.3 Quantum detection efficiency

The quantum detection efficiency (QDE) of the bare part areas of the SUMER MCP's were measured as part of the overall detector characterization. The results presented in Figure 11 show that the efficiencies are slightly lower than expected compared to other bare MCP data[13]. In part this is due to the lack of a grid "retarding mesh" to control the loss of front emitted photoelectrons. However, one distinct anomaly was noted during the scrubbing process that concerned the KBr coated area of the MCP. Flat field data taken at 2537Å prior to scrub (Figure 12) shows that the KBr coated area is about 3x less sensitive than the bare areas. This in itself is not unusual, but the behavior after the scrub presented some curious effects. It was noticed that after scrub the detector background was very high, but that in fact this was entirely due to the photocathode sensing the room lights. Remeasuring the flat field at 2537Å it was clear that the bare areas of the MCP had remained stable, but the KBr was now substantially more sensitive than the bare areas (Figure 12). Thus the KBr photocathodes in all cases had become sensitized! The effect could easily be removed by momentarily exposing the photocathode to air. However, activation also occured even when the MCP detector was turned off, therefore a direct effect of flux on the photocathode is suspected.

We have investigated this phenomenon by measuring the bare MCP and unactivated KBr QDE over a wide range of wavelengths (Figure 13). A KBr photocathode was then activated with a Hg vapor lamp. This process was monitored by periodic checks of the white light senstivity. This showed that the full activation occured in about 3 hours at an input flux of 10^{11} photons cm^{-2} sec^{-1} and that the level of activation saturated after this point and could not be substantially further enhanced. Subsequent measurements of the QDE showed a dramatic increase of the QDE at the long wavelengths (Figure 13). Note that the long wavelength measurements are possible due to the ability to photon count the photocathode response, and the extremely bright laser (6300Å), halogen (4000 - 5500Å) and UV Hg vapor lamp (<3200Å) sources produce large signals on the reference photodiode. The KBr activation seems to be affecting the long wavelengths more than the short. The QDE in the actual bandpass of the KBr (<1600Å) is probably not affected at all. Our initial explanation of this peculiarity is that the high UV flux is causing interstitial metastable energy states within the KBr bandgap to be populated. These have a smaller photoelectric threshold than the KBr bandgap and therefore respond to longer wavelength radiation. We are currently investigating the dynamics of the activation and the implications for other photocathodes, and their use in spaceflight instruments.

4.4 Flat field characteristics

The photocathodes for the UVCS detectors covered the entire detector active area, whereas those for the SUMER detectors were deposited by masking the MCP surface so that only the central region was exposed. The top MCP then required careful alignment within the detector aperture prior to scrub. The contrast enhanced flat field response of the SUMER-1 detector is shown in Figure 14. This is a compilation of two images with over 1.1×10^9 events in total. One image was taken with an Hg vapor lamp (2537Å), and the other with a Resonance[15] Krypton line source (1236Å). The images are combined to bring out the features of both the bare MCP and the KBr photocathode region (center 512 pixels). The KBr has roughly 15 times the bare QDE at 1236Å, whereas at 2537Å, it is the bare MCP that has roughly 3x higher efficiency than KBr (Figure 12). The overlap of these two images produces the contrasted vertical lines at the edges of the photocathode region. Flat field images were acquired at rates of over 150,000 events/sec, and binned into 1024x360 25μm bins, the SOHO flight format.

Typically the dominating modulation is that of the MCP multifibers. MCP modulation at the multifiber boundaries is usually of the order 10%-15%[16]. One unusual feature for the SOHO MCP's is that modulation due to the MCP multifiber structure is not very strong. A single pixel histogram in X, is shown in Fig. 15, and demonstrates the multifiber modulation (≈6% peak-peak) and sub-multifiber modulations. This performance is probably a direct result of the fabrication

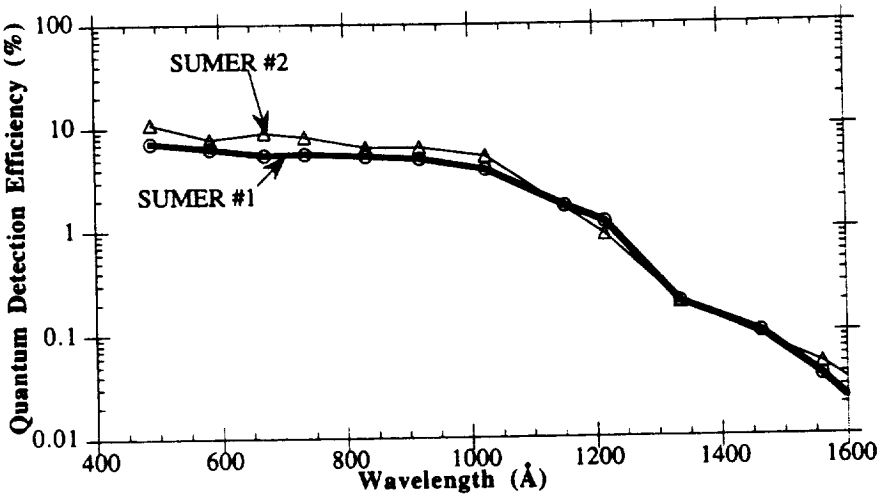

Figure 11. Bare MCP quantum detection efficiencies for the two flight SUMER detectors

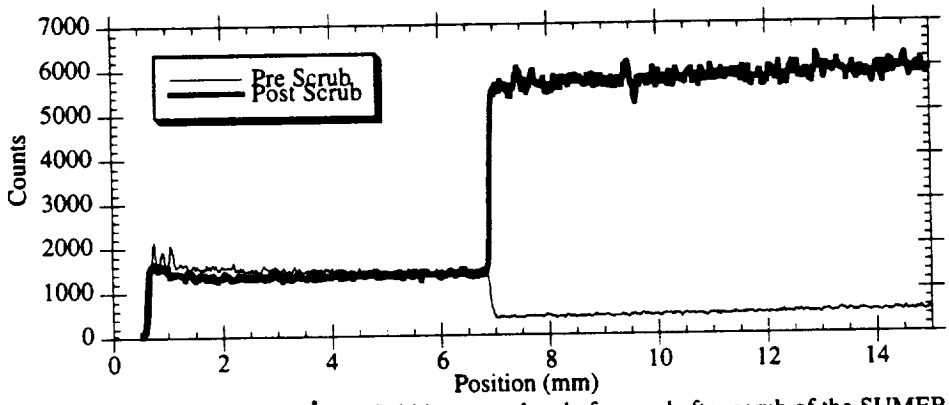

Figure 12. Histogram of 2537Å flat field images taken before and after scrub of the SUMER 2 flight detector showing the enhancement of the KBr QDE after the scrub process.

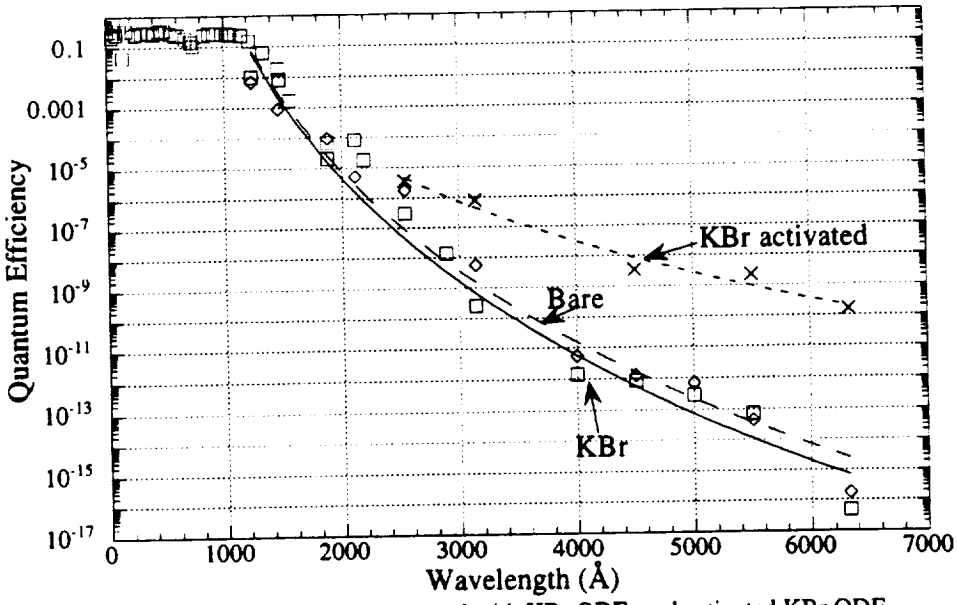

Figure 13. Bare MCP QDE compared with KBr QDE, and activated KBr QDE

process for the entire boule of material from which these MCP's came. Earlier results have linked the MCP multifiber modulation to physical distortions of the MCP pores at the boundaries of the multifibers[16]. A number of dead spots are clearly visible in the flat field image shown in Fig. 14, which are probably due to MCP fabrication defects. A histogram of the statistics of the intensity map of a large ≈3mm x 3mm area of the image is shown in Fig. 16. The intensity variations (σ=3.7%) are larger than would be expected for purely statistical variations for a flat field at this level (σ=1.5%). This is due to the large scale MCP multifiber modulations of the flat field. In comparison, taking a small area wholly inside a multifiber image the intensity variations (σ=2.3%) are much closer to the statistical limit. Even though the overall flat field modulations are relaively small they can produce unwanted effects in high signal to noise observations. Therefore for some observations the spectra will be shifted to average out the modulations[17].

5. Instrument integration tests

The SUMER detectors were integrated into the SUMER instrument at the Max Planck Institute for Aeronomy, Lindau. Upon initial checkout and acceptance of the two detectors, an extensive calibration procedure followed. Collimated light was generated by a gas-discharge source built and operated by PTB. The light output for almost 30 lines was calibrated against the electron storage ring DESY to within ~5%. Light dispersed through the SUMER instrument was collected on the detectors from at rates sometimes approaching 500,000 counts per second. Instrument effective areas were found to agree very well with predicted areas based on sub-system measurements, and detector and instrument properties and functionality were well catalogued. A sample spectrum for nitrogen is shown in Figure 17. During end-end calibrations, several regions of the detectors were spectrally illuminated to such an extent as to have accumulated to well over 1 Coulomb cm^{-2}. These regions showed no permanent gain loss in further testing, including 'on-orbit' flat-fielding techniques, which were performed by scanning a series of Ar lines across the detector during image integration.

The UVCS Ly-α and O-VI detectors were integrated and aligned in the spectrometer at Alenia, Turin. A Kr lamp spectrum taken with the UVCS Ly-α detector on the UVCS spectrograph is shown in Figure 18, demonstrating high signal to noise and low background for the detector. End-end tests of the instrument were also recently successfully performed at the Center for Astrophysics at the Harvard-Smithsonian Astrophysical Observatory in Cambridge, MA. Thus both sets of detectors and their host instruments are on track for the scheduled lauch of SOHO which is due to occur in the late 1995 time frame.

6. Acknowledgments

Many grateful thanks are extended to the many unmentioned people who contributed to this effort at U.C. Berkeley, Lockheed, and the Goddard Space Flight Center. We also thank Prof. K. Wilhelm and the SUMER team members, and Prof. J. Kohl and the UVCS team members. This work was supported by Fairchild contract #SC-00858, and NASA grant NAG5-2304.

7. References

1. The SOHO mission, ESA SP-1104, (1988)
2. Siegmund, O.H.W. E. Everman, J. Vallerga, J. Sokolowski, and M. Lampton, *Applied Optics*, **26(17)**, 3607 - 3614 (1987).
3. Siegmund, O.H.W. and G. Gaines, Proc. SPIE, **1344**, 217-227 (1990).
4. Siegmund, O.H.W. M.A. Gummin, J. Stock, D. Marsh, R. Raffanti, and J. Hull, *Proc. SPIE*, **2006**, 176-187 (1993).

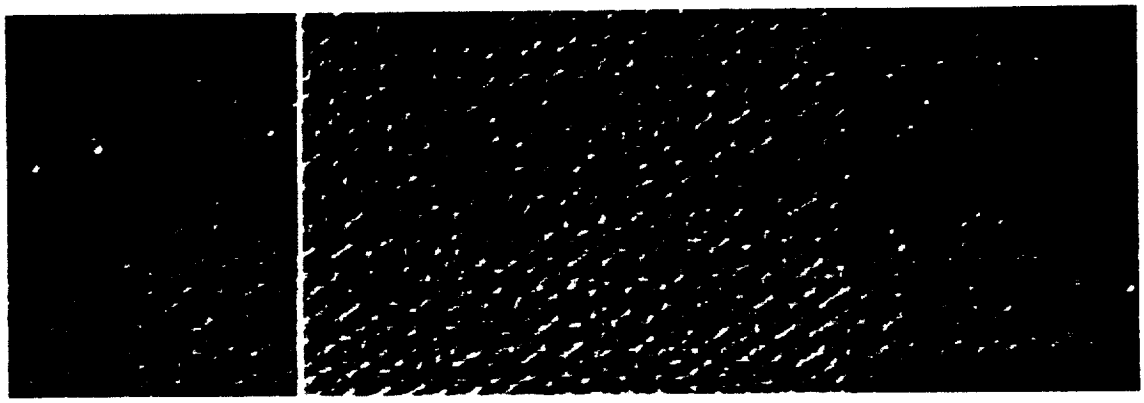

Figure 14. Flat field image at 2537Å &1236Å with $>10^9$ photons taken with the SUMER 1 flight detector. The contrast has been enhanced to show the multifiber modulation. The center area is where a is where a KBr photocathode has been applied. Note several MCP dead spots due to defects.

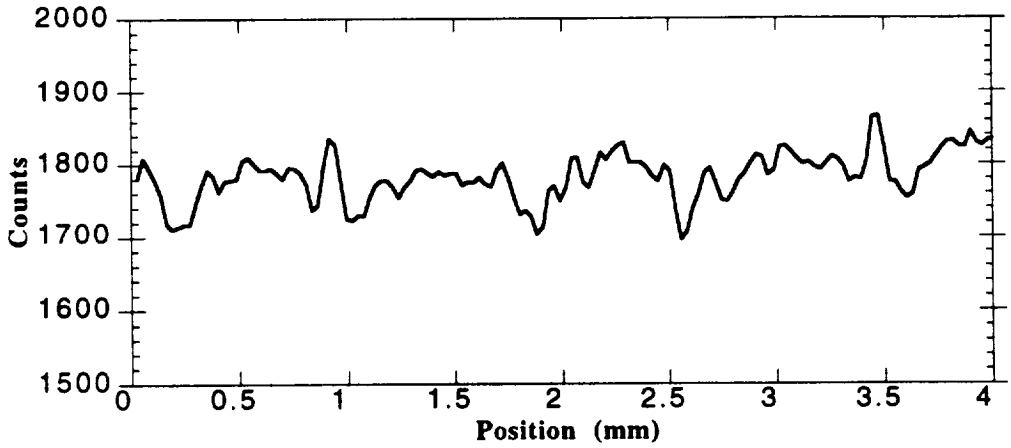

Figure 15. Histogram slice through the image shown in Figure 14. The slice length is ≈5 multifibers long, the multifiber modulation can be seen to have ≈6% modulation peak-peak (≈1% RMS)

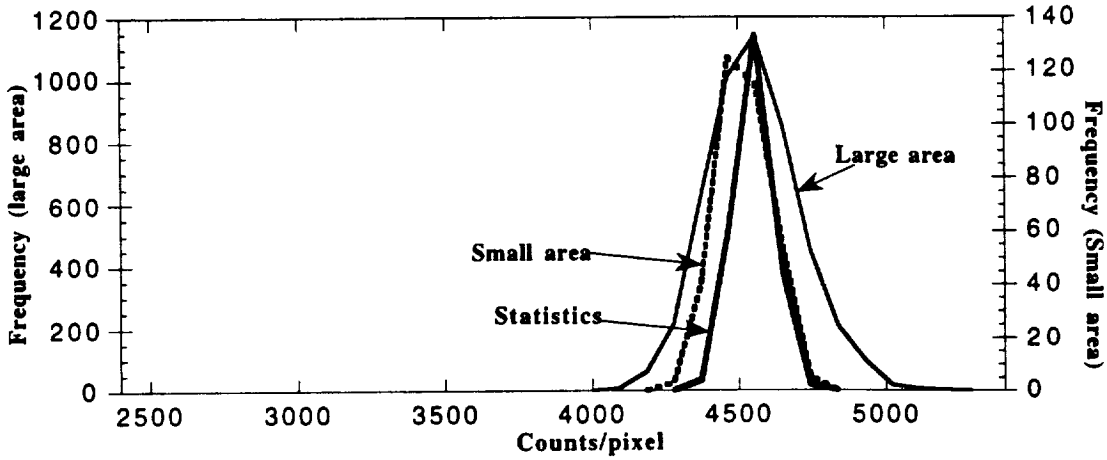

Figure 16. Flat field intensity variations for an area of many multifibers (σ=3.7%) and an area smaller than a multifiber (σ=2.3%) , compared with the expected statistical variations (σ=1.5%)

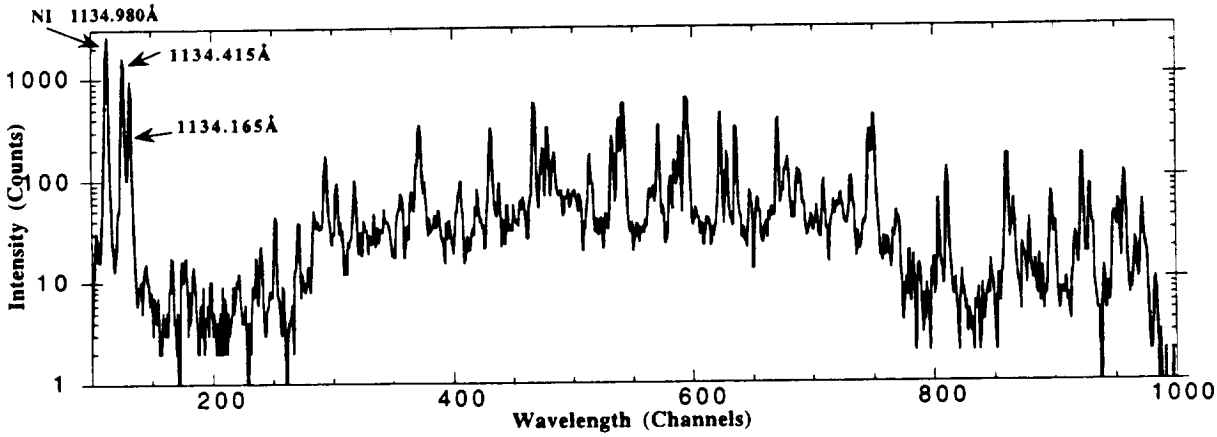

Figure 17. SUMER calibration spectrum showing a high resolution spectrum of nitrogen.

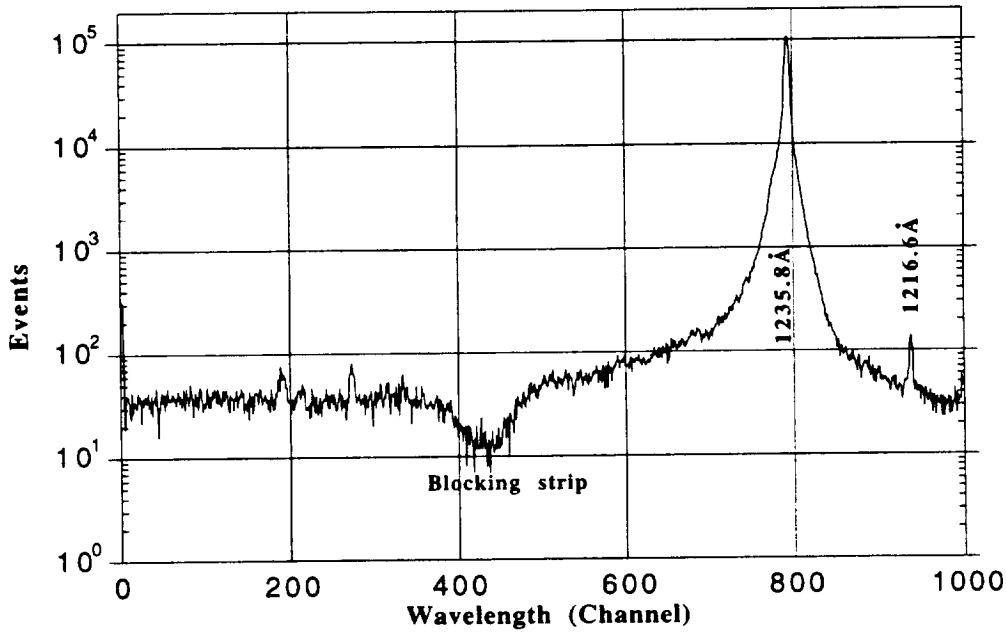

Figure 18. UVCS Kr lamp calibration data showing the Kr 1236.8Å line, Lyα 1216.6Å contamination, and the detector background level under the Lyα detector blocking strip.

5. Siegmund, O.H.W. M.A. Gummin, J. Stock and D. Marsh, ESA symposium on detectors, **ESA SP-356**, 89-96, December 1992.
6. Siegmund, O.H.W., Vallerga, J., and Wargelin, B., *IEEE Trans. Nucl. Sci.* , **NS-35,** 524 (1988).
7. Fraser, G.W., Pearson, J.F., and Lees, J.E., *Nucl. Instrum. & Meth.*, **A254**, 447 (1987).
8. Slater, D.C., and J.G. Timothy, *Proc. SPIE*, **1549**, 68 (1991).
9. Siegmund. O.H.W., and J.Stock, *Proc. SPIE*, **1549**, 81-89 (1991).
10. Fraser, G. W., Pain, M.T., Lees, J. E., Pearson, J. F., *Nucl. Instrum. & Meth. A,* preprint (1991).
11. Siegmund, O. H. W., 1989, *Proc. SPIE*, **1072**, 111-118.
12. Panitz, J. A. and Foesch, J. A. *Rev. Sci. Instrum.* **47**, 44 (1976).
13. Siegmund, O.H.W., K. Coburn, and R.F. Malina, *IEEE Trans. Nucl. Sci.* **NS-32**, 443-447 (1985).
15. Resonance, Ltd. Ontario, Canada.
16. Vallerga, J.V., Siegmund, O.H.W., Vedder, P.W., Gibson, J., *Nucl. Instrum. & Meth.* **A310**, 317-322 (1991).
17. Sahnow, D. J., C. W. Bowers, O. H. W. Siegmund, J. Stock, and M. A. Gummin, *Proc. SPIE*, **1945**, (1993).